Retrogression, reaging, and mechanical behaviour of a 1441 Al–Li–Cu–Mg–Zr alloy

Article *in* Zeitschrift für Metallkunde · December 2005

DOI: 10.3139/146.101193

3 authors, including:

Uday Chatterjee
Indian Institute of Technology Kharagpur
122 PUBLICATIONS **1,273** CITATIONS

SEE PROFILE

K. S. Ghosh[a], K. Das[b], U. K. Chatterjee[b]
[a] Department of Metallurgical and Materials Engineering, National Institute of Technology, Warangal, India
[b] Department of Metallurgical and Materials Engineering, Indian Institute of Technology, Kharagpur, India

Retrogression, reaging, and mechanical behaviour of a 1441 Al–Li–Cu–Mg–Zr alloy

A 1441 Al–Li–Cu–Mg–Zr alloy was subjected to retrogression treatment and the retrogressed states were immediately reaged to various tempers. Hardness measurement, tensile testing, and SEM fractography have been carried out to conventional peak-aged, retrogressed, retrogressed and reaged (RRA), and over-aged tempers of the alloy. Retrogression treatment applied to peak-aged tempered alloys resulted in a decrease in hardness and tensile strength, an increase of ductility, and a serration phenomenon in the plastic region. These are primarily due to the dissolution of matrix strengthening δ′ precipitates into solid solution upon retrogression treatment. Retrogressed states have been reaged to various under-, peak-, and over-aged tempers. Reaging the retrogressed state to peak-aged temper has resulted in attaining the original peak-aged strength and ductility value. SEM fractography study has been carried out and fracture surfaces exhibited predominantly intergranular fracture in presence of few dimples. TEM and DSC studies have been carried out to observe the microstructural changes upon RRA treatment and to explain the mechanical behaviour of the alloy.

Keywords: Retrogression and reaging (RRA); 1441 Al–Li–Cu–Mg–Zr alloy; DSC; Tensile properties; SEM fractographs

1. Introduction

Al–Li alloys are candidate materials for aerospace industries because of their reduction in density, increase in elastic modulus and increase in specific strength over the most widely used conventional aluminum base alloys. Al–Li alloys have unattractive fracture behaviour, especially poor ductility and high anisotropy of non-recrystallized products, and are also susceptible to stress corrosion cracking (SCC) in the peak-aged temper [1–6].

The low ductility and toughness of Al–Li alloys are due to many concurrent and many mutually competitive factors involving (i) inhomogeneous nature of slip resulting from coherent ordered δ′ precipitates, (ii) presence of coarse equilibrium δ precipitates at the grain boundaries inducing further strain localization and promoting intergranular failure, (iii) segregation of tramp elements such as sodium, potassium, and sulphur to the grain boundaries. However, for commercial alloys, slip can be homogenized by introducing (i) dispersoids (Al_3Zr), with the addition of zirconium, (ii) semicoherent/incoherent precipitates, such as T_1 (Al_2CuLi), and S (Al_2CuMg), through copper and magnesium additions. Addition of copper and magnesium also reduces the precipitate-free zone (pfz) near the grain boundaries. Thermomechanical processing, duplex aging tempers, retrogression, and reaging (RRA) treatments also optimize the best combinations of tensile properties and toughness [1–7].

A non-conventional two-stage heat treatment process, called retrogression and reaging (RRA) was initially devised by Cina et al. [8, 9] for improving the stress corrosion cracking (SCC) behaviour of 2XXX series aluminium base alloys. It has been found that RRA treatment improves the SCC resistance to 2XXX series as well as for 7XXX and 8XXX series alloys [10–12]. RRA treatment is applied to the alloy of peak-aged temper and involves heating for a short time at a temperature above the artificial aging temperature but around the solvus line of the matrix strengthening precipitates, followed by reaging to the condition similar to that of the original peak-aged temper. Whereas the mechanical behaviour of the Al–Li–Cu–Mg alloys of conventional tempers are studied in detail [13–15], the knowledge about the influence of RRA treatment on the mechanical properties of the alloy is scanty. This paper deals with the investigations on the influence of aging tempers, retrogression, and RRA treatment on hardness, tensile properties and fracture characteristics of a 1441 Al–Li–Cu–Mg–Zr alloy. TEM and DSC studies have been carried out to observe the microstructural changes upon RRA treatment and to explain the observed mechanical behaviour of the alloy.

2. Experimental

A 1441 (Russian grade) Al–Li–Cu–Mg–Zr alloy was used in sheet form having thickness 2.0 mm. The alloy sheet was solutionised at 530–535 °C, water quenched, stretched by 1.5–2.5 %, followed by artificial aging at 150 °C for 4 h and at 170 °C for 24 h corresponding to the peak-aged, T8 temper. The as-received T8 temper sheet was aged at 170 °C for 96 hours to produce over-aged T7 temper. The chemical composition (weight %) of the alloy is given in Table 1. Figure 1 shows the optical micrograph

Table 1. Chemical compositions of the 1441 alloy (wt.%).

Alloy	Al	Li	Cu	Mg	Zr	Fe	Si
1441	Balance	1.9	2.0	0.90	0.09	0.11	0.05

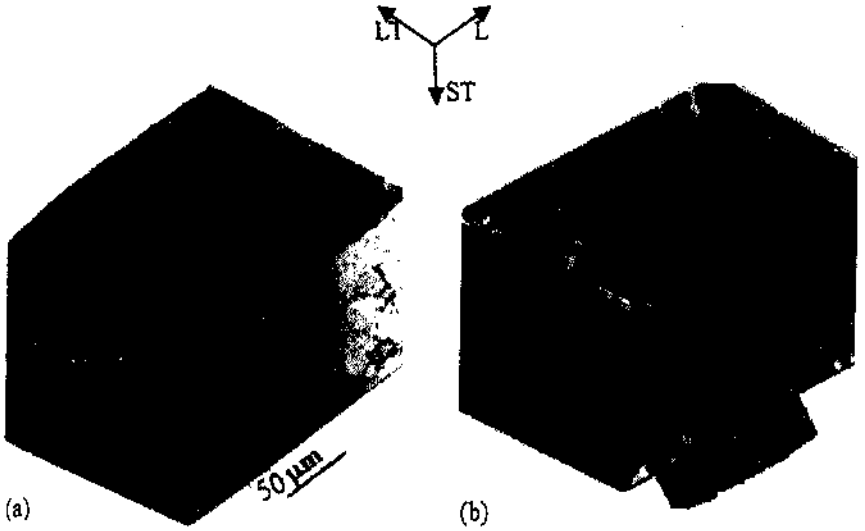

Fig. 1. Triplanar (a) Optical and (b) SEM micrographs of the 1441-T8 temper.

of the as-received 1441-T8 temper alloy. The triplanar micrographs, Fig. 1, show that the grains are more or less equiaxed in all the three longitudinal (L), long transverse (LT), and short transverse (ST) directions of the sheet. The grain size of the alloy was found to be of the order of 15–20 μm, on average.

RRA treatments applied to the as-received alloy sheet were carried out in a vertical tube furnace in air. The retrogression temperatures were chosen above and below the δ' solvus line of the Al–Li phase diagram. After a precise time of holding the samples in the furnace, specimens were released and quenched into ice-cold water followed by reaging to various tempers. Retrogression and reaging (RRA) schedule adopted are given in Table 2.

For transmission electron microscopy (TEM) studies, the specimens were mechanically thinned to a thickness of approximately 100 μm, punched to get a 3 mm disc and finally thinned down to perforation using a Fischione twin-jet electropolisher, operating at 25 volts and 2.5 amps current, in an electrolyte of composition 30 % HNO_3 and 70 % CH_3COOH at a temperature of approximately −20 °C. A Philips CM12 was used for the observation of the microstructures. For differential scanning calorimetry (DSC) studies, specimens of approximately 30 mg were cut from the coupons of various tempers of the alloy and the sides of the specimens were made absolutely flat and smooth for a good contact with the crucible. DSC runs were initiated from room temperature to approximately 500 °C at a heating rate of 10 K/min in an argon atmosphere, using a Stanton Redcroft Model STA 625 simultaneous thermal analyzer. The output, viz. the net heat flow to the reference (high-purity annealed aluminum) relative to the samples, was recorded as a function of temperature.

A Vickers hardness machine was used for hardness measurement. For tensile testing (tensile axis transverse to rolling direction; unless otherwise specified) with dimensions of 20 mm extended gauge length, 4 mm width and 1.8 mm thickness were obtained from the sheet. The surfaces of the specimens were ground to 100 μm minimum so as to remove the lithium- and magnesium-depleted zones and subsurface porosity zones developed during solutionising at temperature 535 °C and subsequent treatment carried out in air [16]. The gauge portions of the specimen surfaces were polished in emery papers lubricated with kerosene oil up to 600 grits and finally cleaned and de-oiled by rinsing in acetone. Tensile testing was at a strain rate of $1.33 \times 10^{-3}\ s^{-1}$ using INSTRON universal testing machine. Tests are repeated to confirm results. Fracture surfaces of broken tensile specimens were observed using SEM (JEOL, JSM-5800), Japan.

Table 2. Retrogression and Reaging (RRA) schedule applied to the as-received 1441-T8 temper alloy.

Samples for studies	Retrogression temperature and time	Reaging schedule	RRA temper designation
Hardness	At 215, 230, 250 and 270 °C for 1 to 40 min	Isothermal reaging (IA) at 170 °C for 2, 26 and 96 h corresponding to under-, peak-, and over-aged tempers	–
TEM and DSC and tensile testing	At 230 °C for 15 min	Isothermal reaging (IA) at 170 °C for 26 h	1441R230IA
		Duplex reaging (DA) at 150 °C for 36 h, followed by heating to 190 °C at a rate of 5–7 K/min and holding for 1 h at the temperature	1441R230DA
	At 270 °C for 5 min	Isothermal reaging (IA) at 170 °C for 26 h	1441R270IA
		Duplex aging (DA) at 150 °C for 36 h, followed by heating to 190 °C at rate of 5–7 K/min and holding for 1 h at the temperature	1441R270DA

3. Results and discussion

3.1. TEM microstructure

Figures 2a–d, show a few representative TEM bright-field images of the peak aged T8, RRA, and T7 tempers of the alloy, exhibiting T_1, S′, δ′, and δ phases that are present in the alloy system. Diffraction patterns of the phases have not been taken and also the precipitation mechanisms of these phases are not discussed here as these are well established for the alloy system [17–20]. In fact, attention has been focused to observe the changes in microstructural features, i. e. the size, distribution, and morphology of the phases upon retrogression and RRA treatment. Figure 2a (T8 temper) exhibits uniformly distributed grains of fine T_1 and S′ phases. The micrograph also shows that in one of the grains preferential heterogeneous precipitation of these phases along dislocations has taken place. Equilibrium δ phase is also visible at the grain boundaries. Figure 2b (1441R270DA, RRA temper) shows uniform distribution of matrix-strengthening δ′ precipitates. TEM studies have been carried out to retrogressed (1441R230) temper also, but neither in bright-field nor in dark-field images of the δ′ precipitates (as there were no superlattice spots) could be seen. This confirms that retrogression treatment dissolves the δ′ precipitates into solid solution. DSC studies have also confirmed the dissolution of δ′ precipitates into solid solution upon retrogression treatment which will be discussed in the next section. Further, retrogression treatment results in a decrease of dislocation density as observed by the authors in the 8090 Al–Li–Cu–Mg–Zr system and also reported in literature [21]. Figure 2c exhibits uniformly distributed precipitation of T_1 and S′ phases within the matrix for the 1441R230DA RRA temper. Figure 2d (over-aged T7 temper) exhibits uniform distribution of fine T_1 and S′ phases within a grain and preferential heterogeneous precipitation of these phases at dislocations. Equilibrium δ phase is also visible along the high-angle grain boundaries. The δ phase is larger in size as compared to that of the T8 temper (Fig. 2a), which is obvious because it is an established phenomenon that the relative amounts and size of the equilibrium δ phase increase with aging time because the transformation δ′ (Al_3Li) → δ (AlLi) occurs during the aging process. From the photomicrographs in Figs. 2a, 2c, and 2d, it can be concluded that the distribution and morphology of the T_1 and S′ phases do not change much upon RRA treatment as also stated in the literature and found in the 8090 Al–Li–Cu–Mg–Zr alloy [22].

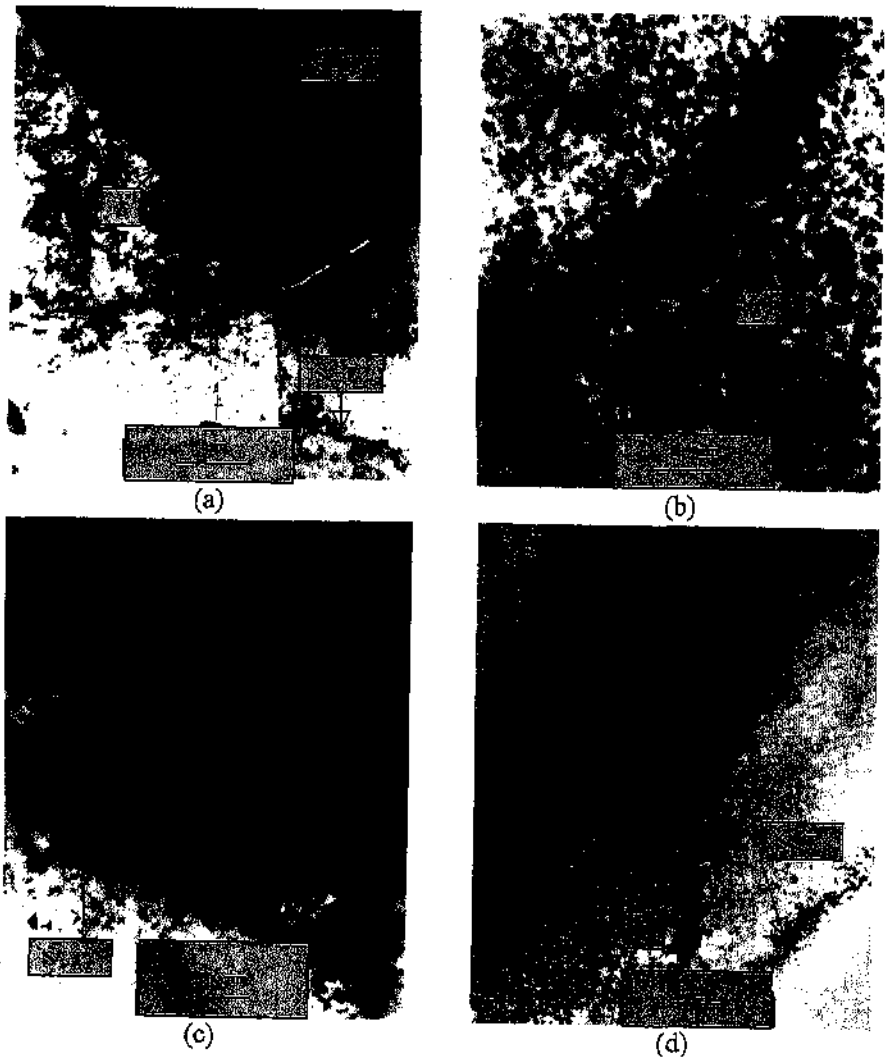

Fig. 2. TEM micrographs for (a) T8 temper exhibiting grain containing T_1 and S′ phases uniformly distributed and in one of the grains heterogeneously precipitated along the dislocations. Equilibrium δ phase is seen along the grain boundaries, (b) 1441R270DA temper shows δ′ phase uniformly distributed within the matrix, (c) 1441R230DA temper displays uniform and widespread distribution of T_1 and S′ phases, and (d) T7 temper shows T_1 and S′ phases uniformly distributed within a grain and heterogeneously precipitated along dislocations and equilibrium δ phase along the high-angle grain boundaries.

3.2. DSC thermograms

Figures 3a–d show the DSC thermograms of the 1441 alloy of various tempers. Figure 3a (solution-treated and water-quenched state) exhibits many exothermic and endothermic peaks (marked with letters A to F) indicating the sequence of precipitation and dissolution reactions. The precipitation reactions are (A): formation of GPB zones and precipitation of the δ′ phase, (B): precipitation of δ′ phase, (C): dissolution of GPB zones and δ′ precipitates, (D): precipitation of S (S′), T_1, and δ phases, (E): dissolution of S (S′), T_1, and δ phases, and (F): dissolution of Li-bearing zone. The results are in close agreement with the literature [23–26]. The peak region B corresponding to the precipitation of δ′ phase for this Al–Li alloy, is not clearly resolved with a sharp peak, as the precipitation of the δ′ phase has occurred at lower temperature resulting in overlapping with the peak A region. The possible reasons of precipitation of the δ′ phase at lower temperature has been discussed elsewhere [27]. Figure 3b (T8 temper) displays two clear endothermic peak regions C (dissolution of GPB zone and δ′ phase) and E (dissolution of S′ (S), T_1, and δ phases) and exothermic peak region D (precipitation of S′ (S), T_1, and δ phases). The absence of peaks A and B in the thermogram of T8 temper is obvious as the solid solution is not supersaturated with solute atoms or, in other words, the matrix contains equilibrium amounts of δ′ precipitates. In the peak region D, two distinct peaks, D_1 and D_2, indicate that the precipitation of S′, T_1, and δ phases do occur at different temperatures in the T8 state as compared to that occurred in the as-quenched condition because of the difference of level of supersaturation of solutes. Figure 3c (retrogressed 1441R230 state) shows the appearance of low-temperature exothermic peaks A (i. e. formation of GPB zones) and B (i. e. δ′ precipitation) which is obvious because the solid solution is supersaturated with Li atoms. Hence, it can be concluded that retrogression causes dissolution of δ′ phase. Figure 3d (1414R230DA RRA temper) also exhibits two endothermic peak regions C and E and an exothermic peak region D, similar to that of the T8 temper (Fig. 3b), indicating that the microstructural features, i. e. the type of phases and precipitates, are similar to that of the T8 temper.

3.3. Retrogression and hardness

Figure 4 shows the variation of hardness with retrogression time at the retrogression temperatures 215, 230, 250, and 270 °C. The graphs exhibit the characteristic shape of retrogression phenomenon of the T8 temper of the alloy. The hardness vs. retrogression time curves have two distinct re-

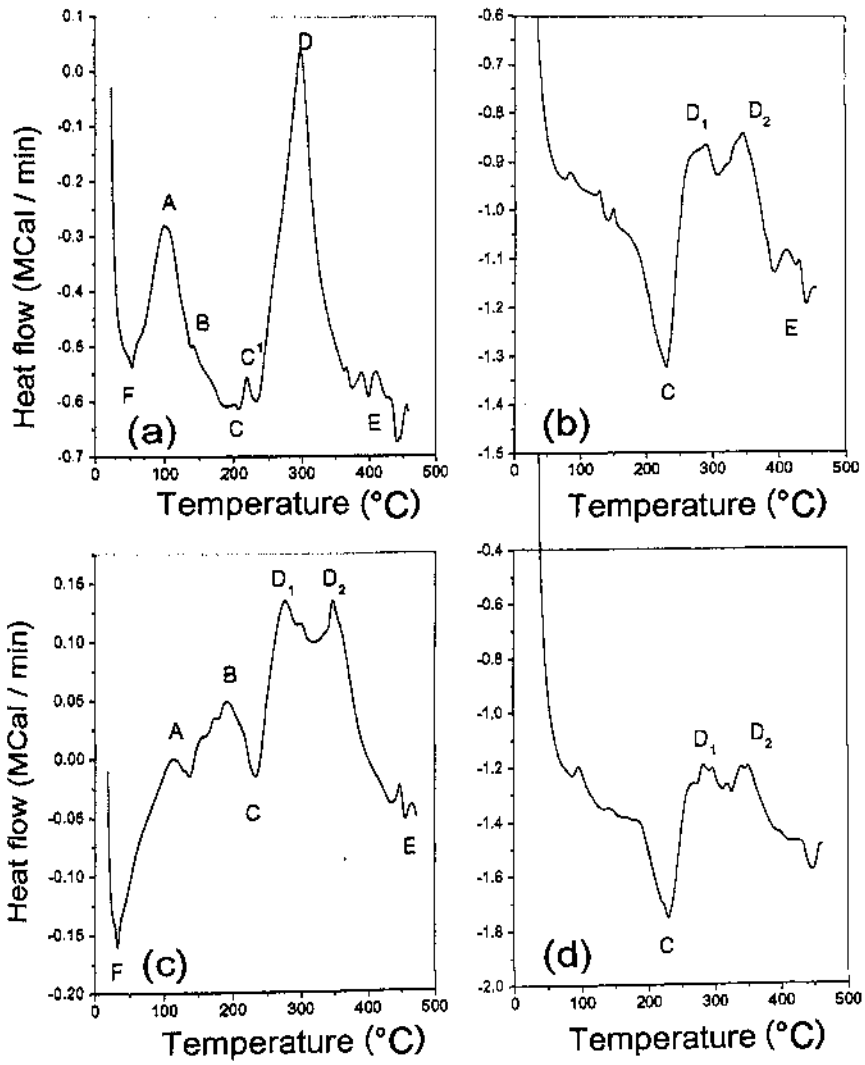

Fig. 3. DSC thermogram of (a) solution-treated and water-quenched, (b) T8, (c) 1441R230, and (d) 1441R230DA tempers of the 1441 alloy at a heating rate of 10 K/min.

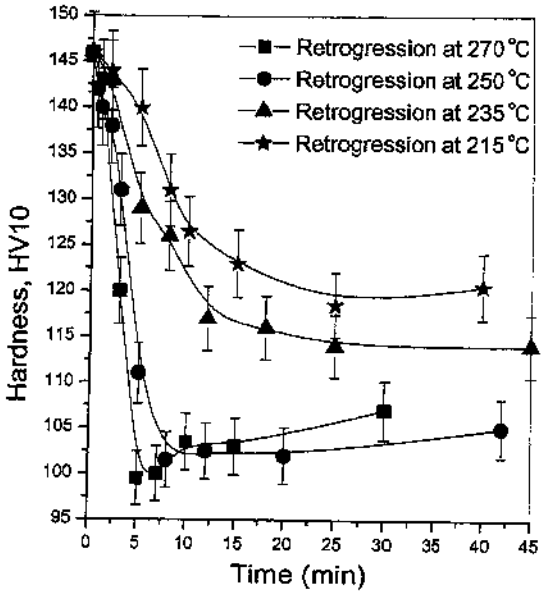

Fig. 4. Variation of hardness with retrogression time of the 1441-T8 alloy.

gions: (i) an initial sharp decrease in hardness, (ii) attainment of a minimum followed by a slight increase in hardness after which there is no further change in hardness values for the retrogression time studied. The trends of the results are in accordance with the results of 7XXX and 8XXX alloy series reported by various researchers [28–32]. However, the observed retrogression time corresponding to minimum hardness is different from that reported in literature [33] as this depends on many variables such as sheet thickness, heating medium, etc. [34]. The decrease of hardness with retrogression time is due to the preferential dissolution of the coherent matrix strengthening δ' precipitates which are no longer stable at the retrogression temperature. TEM and DSC studies have confirmed the dissolution of δ' precipitates into solid solution. During retrogression, other precipitates like T_1, S', S remain mostly undissolved, but the growth of the Li-bearing phases, particularly δ and T_1, occurs. Further, the decrease of hardness upon retrogression treatment is also attributed to the decrease of dislocation densities [22, 32]. With the increase of retrogression temperature, the rate of hardness drop increases, the minimum hardness value decreases, and the retrogression time to reach the minimum hardness decreases as well. This is consistent with the concept of higher disso-

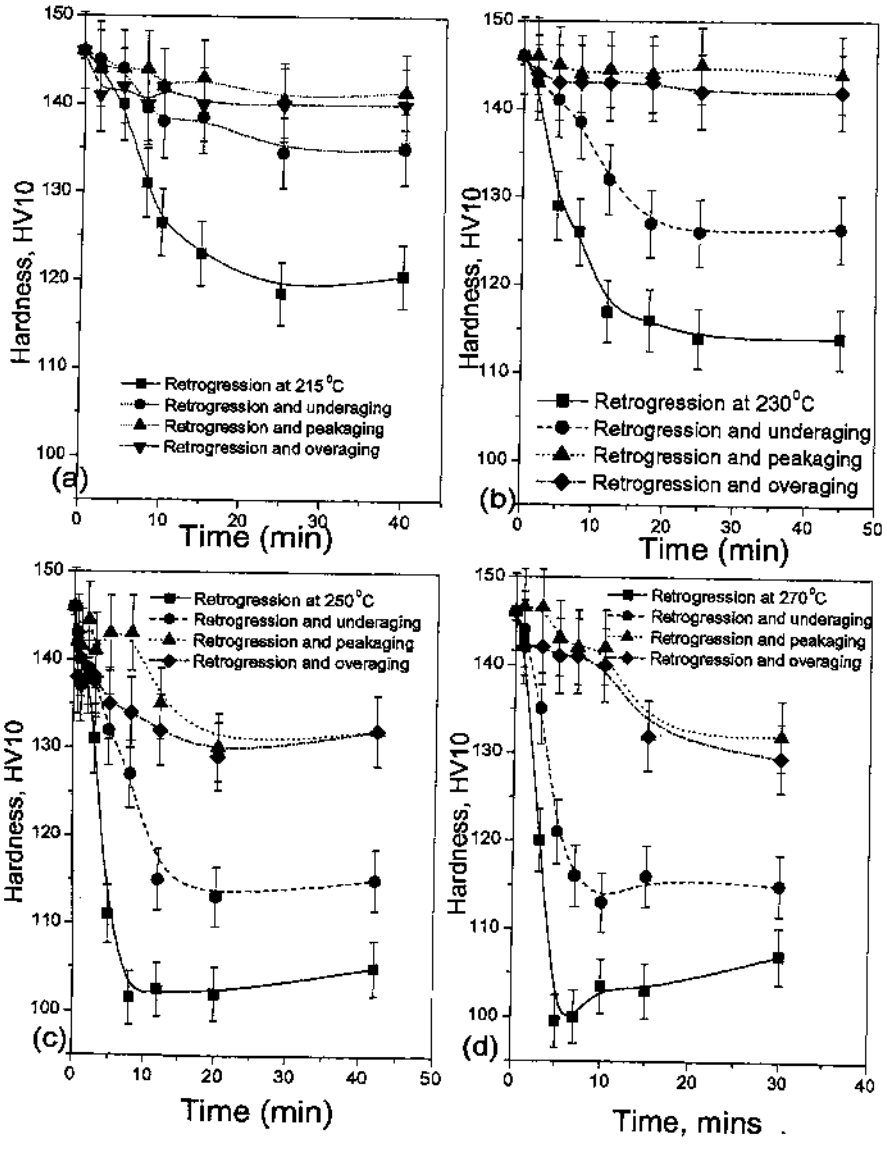

Fig. 5. Variation of hardness with retrogression time and reaging to different tempers of the 1441 alloy.

lution rate with increasing temperature of retrogression. The minima in the retrogression curves are indicative of the maximum dissolution of the δ' precipitates. Complete dissolution of δ' is not possible. Initially, the rate of dissolution is higher than the precipitation. But at the minima of the curves for all the temperatures, the rate of dissolution is equal to the rate of precipitation. The slight increase of hardness after the minima is due to the onset of a structural age-hardening effect.

3.4. RRA and hardness

Figures 5a–d show the variation of hardness with retrogression time at a given retrogression temperature and also the change in hardness on subsequent reaging the retrogressed state to under-, peak-, and over-aged tempers. Reaging the retrogressed tempers leads to a regain of hardness which is attributed to the reprecipitation of δ' within the matrix that has been shown by TEM and DSC studies. Reaging the retrogressed state to peak-aged temper has caused regaining the initial T8 temper hardness. However, retrogression for longer time compared to the time of the minimum hardness and reaging to peak aged tempers failed to achieve the T8 hardness. This is due to the fact that longer retrogression time and higher retrogression temperatures led to over-aged T7 state. At all the retrogression temperatures, the hardness values of retrogression and under-aged (RUA) tempers are lower than the hardness values of the retrogression and over-aged (ROA) tempers which are again lower than the hardness values of the retrogression and peak-aged (RRA) tempers. The reason is that in the under-aged tempers the reprecipitation of matrix strengthening δ' precipitates is not complete, whereas in the peak aged tempers reprecipitation of the δ' precipitates is complete giving rise to maximum hardness and, in the over-aged tempers, to the growth of the precipitates. Kanno et al. [31] have suggested that RRA is effective only for alloys containing coherent dispersoids, such as 8XXX. This is why RRA T77 treatment is effective in this alloy containing zirconium that produces β' (Al_3Zr) coherent dispersoids.

3.5. RRA and tensile properties

Figure 6 exhibits the representative stress–strain curves of the 1441 alloy of T8, retrogressed 1441R230 and 1441R270, 1441R230UA RUA, 1441R230DA, and 1441R270DA RRA tempers, tested in an INSTRON universal testing machine at a strain rate of $1.33 \times 10^{-3}\ s^{-1}$. Plastic region of stress–strain curves for the retrogressed and RUA tempers exhibiting discontinuous yielding are shown separately for better clarity as an inset. The average tensile properties of the alloy of various tempers are given in Table 3.

Figure 6 shows that the retrogressed tempers have lower yield and ultimate tensile strength and higher ductility compared to that of the T8 and RRA tempers. The higher the retrogression temperature the more is the decrease of strength values and the more pronounced is the ductility. The strength and ductility values of the 1441R230UA RUA temper are higher than those of the retrogressed 1441R230 and 1441R270 tempers but are lower than those of the T8 and RRA tempers. The improvement of ductility values in the retrogressed tempers is due to better slip

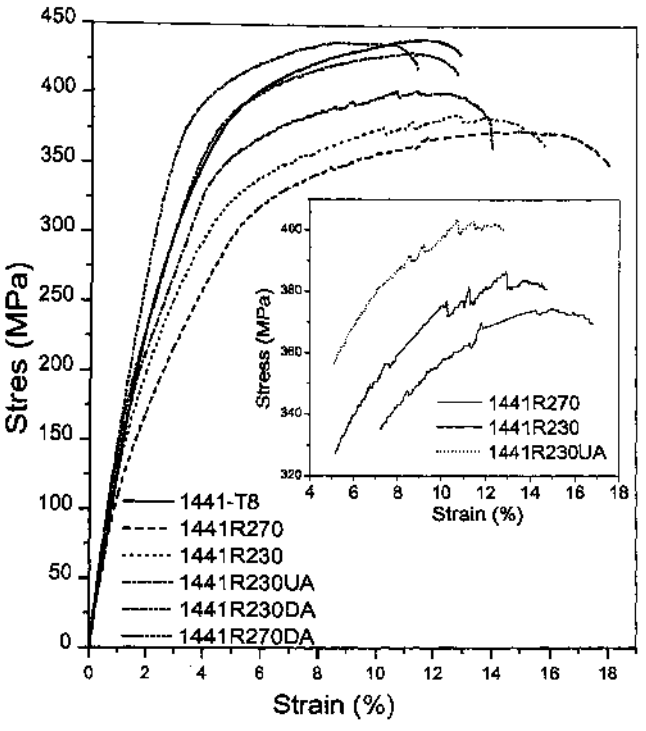

Fig. 6. Stress–strain curves of the 1441 alloy of various tempers tested at a strain rate of $1.33 \times 10^{-3}\ s^{-1}$.

homogenisation and transition from coarse planar to homogeneous deformation because of the absence or low volume fraction of coherently ordered δ' precipitates in the matrix that control the deformation mode. The tensile properties of the RRA tempers are in the same range as those of the T8 temper. Reaging the retrogressed tempers to peak-aged temper causes complete reprecipitation of δ' phase in the matrix and thus leading to regaining the initial T8 tensile properties. Reaging to under-aged temper causes partial reprecipitation δ' phase and that is why the strength values of the RUA tempers are lower than those of the T8 and RRA tempers but higher than those of the retrogressed temper. In this regard, it is to be highlighted that although the tensile properties of the RRA tempers are in the same range as those of the T8 temper, the total aging time of the RRA tempers is almost twice that of the conventional T8 temper and hence microstructural features of the RRA tempers approach those of the T7 temper [22].

Table 3. Average values of tensile properties of the 1441 alloy of various tempers tested at a strain rate of $1.33 \times 10^{-3}\ s^{-1}$.

Alloy temper	YS (MPa)	UTS (MPa)	Plastic strain to fracture ε_p (%)
1441-T8 (Longitudinal)	385	432	8.74
1441-T8	395	447	8.00
1441R230	330	387	11.50
1441R270	325	374	12.39
1441R230UA (170_2)	350	404	9.15
1441R270UA (170_2)	355	412	9.65
1441R230IA	390	443	7.75
1441R270IA	380	440	7.80
1441R230DA	400	449	8.05
1441R270DA	390	442	8.15
1441-T7	380	430	7.50

Discontinuous yielding has been observed in the plastic region of the stress–strain curves of the retrogressed and RUA tempers. But there is no such occurrence of discontinuous yielding or serration in the T8, RRA, and T7 tempers. The occurrence of plastic instabilities in the retrogressed 144R230 and 1441R270, and RUA states might result from a negative value of the microscopic (local) strain-hardening rate (type h instability) or from negative microscopic strain-rate sensitivity of the flow stress (type S instability) [35–38]. The onset of serrated yielding after a finite plastic strain is associated with a transition from positive to negative strain-rate sensitivity as strain (or stress) increases. In the first hypothesis, these instabilities arise from work softening due to slip localization (or planar slip); the shearing of the δ′ precipitates probably promotes the localization of deformation, as suggested by many authors [39, 40]. In the second hypothesis, instabilities arise from the interaction between the diffusing solute atoms, viz. Cu, Mg, and mobile dislocations [41–43]. This interaction results in dynamic strain aging, whose macroscopic manifestation is the Portevin–Le Chatelier effect. If the above mentioned hypothesis holds good for the occurrence of plasticity in retrogressed tempers, then it is also an indication that retrogression treatment causes reversion of δ′ precipitates into solid solution.

3.6. SEM fractography

The monotonic fracture surfaces are helpful in explaining microstructural effects on the ductility and fracture properties of the alloy. Figures 7a–g show the SEM fractography of the alloy of peak-aged T8, retrogressed, retrogressed and reaged (RRA) T77, and over-aged T7 tempers. Extensive fractography of the tensile samples revealed cracking along grain boundaries or intergranular failure, sub-intergranular failure along the subgrain boundaries, and the presence of few dimples.

The mechanism of intergranular cracking in Al–Li–Cu–Mg–Zr alloy has been discussed in detail by Srivatsan [44]. In the peak-aged, and RRA temper conditions, the presence of coherent shearable δ′ precipitates leads to inhomogeneous slip causing severe strain localization during deformation [45, 46]. The inhomogeneous slip causing strain localization is because of the interactions of mobile dislocations with the ordered coherent and partially coherent particles dispersed in the matrix. In an alloy strength-

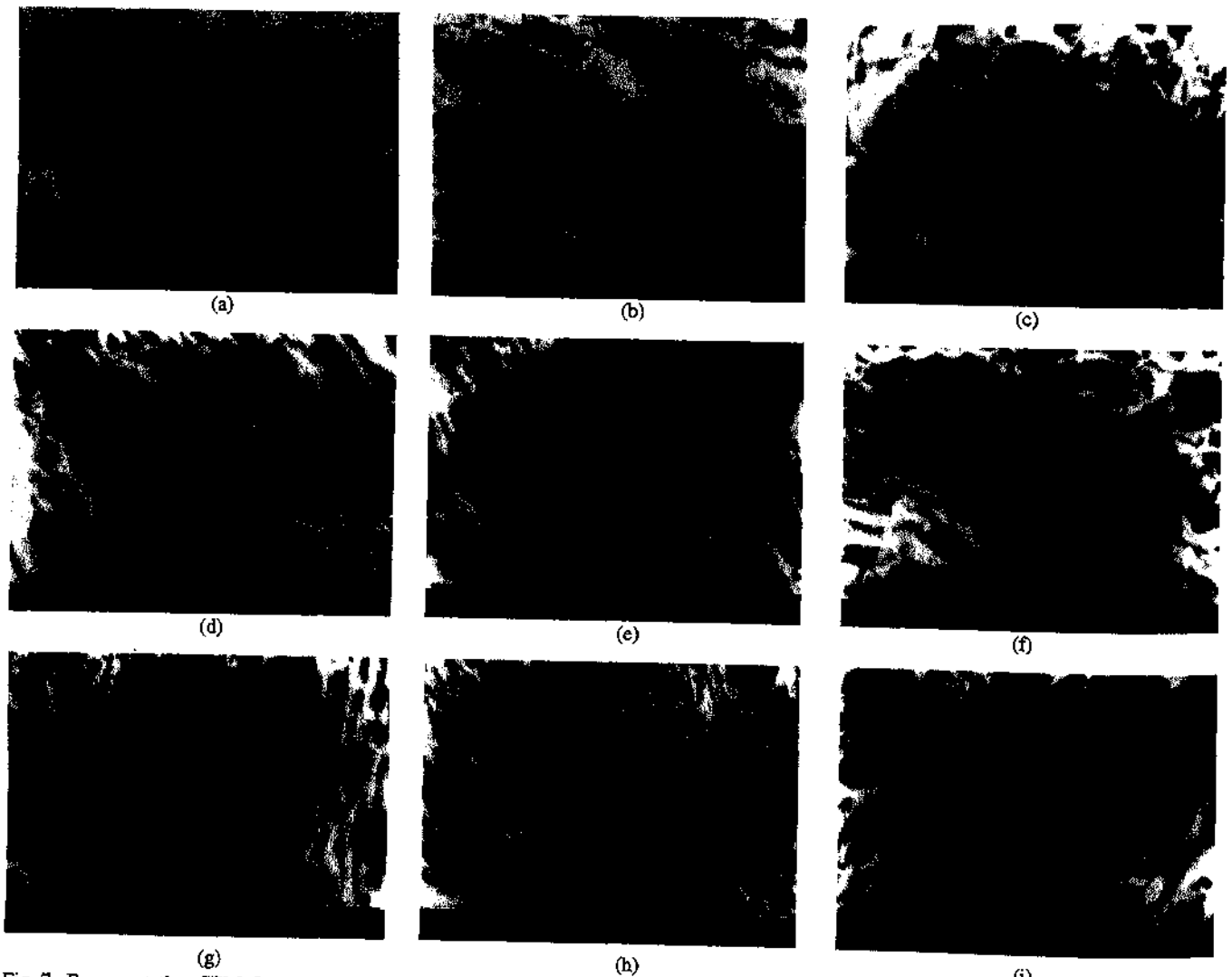

Fig. 7. Representative SEM fractographs of (a) 1441-T8 (longitudinal), (b) 1441-T8, (c) 1441R270, (d) 1441R230, (e) 1441R270UA, (f) 1441R230UA, (g) 1441R270DA, (h) 1441R230DA, and (i) 1441-T7 tempers, showing intergranular and subintergranular failure and the presence of few dimples.

ened by coherent particles, the tendency of strain localization into bands is due to the fact that a dislocation pile ups can shear through the particle more easily than can individual dislocations. In the alloy strengthened with ordered precipitates, the dislocations move as pairs; the first dislocation creates disorder and the second dislocation restores order [47]. During deformation, the dislocations easily shear the ordered coherent and partially coherent precipitate particles, e.g. δ', T_1, S', while moving in close-packed {111} planes in the close-packed directions, resulting in disorder in the form of an antiphase boundary (APB). Once the particles are disordered and slip has occurred on one plane, the area of the APB is decreased, thus favouring additional deformation on the plane [48]. Coarse planar slip bands are resulting. The concentration of deformation in planar slip bands leads to strain localization at the point of their impingement on grain boundaries. The localized planar deformation produces large strain concentration [32]. The increased strength of the age-hardened matrix in the peak-aged condition renders nucleation of flow across the boundary difficult. This effect coupled with the presence of grain boundary precipitates results in enhanced deformation along the grain-boundaries and concomitant low ductility as compared to conventional aluminum alloys of comparable strength. Void initiation results at the intersection of a slip band and coarse grain boundary precipitates. The applied stress assists the growth of voids. Linking of similar voids is an additional factor that promotes and/or enhances intergranular fracture.

Fracture surfaces of specimens of retrogression treatments (Figs. 7c and 7d) also show intergranular cracking and also few dimples are seen. The strain localization by coherent shearable δ' matrix precipitation is less operative in the retrogressed temper as the microstructure has very low volume fractions of δ' precipitates. But the strain localization due to the presence of the grain boundary δ precipitates remains operative and thus the initiation of microvoids near the grain-boundaries leads to intergranular cracking [44, 49].

In the over-aged tempers (Fig. 7i), as usual, the intergranular fracture is prominent, as in addition to the development of strain localizations at the grain boundaries due to the presence of δ', the presence of a considerable amount of equilibrium δ precipitates at the grain boundaries contributes further to the initiation of microvoids near the grain boundaries.

4. Conclusions

TEM photomicrographs and DSC thermograms of the 1441 alloy have exhibited all the probable phases, such as δ' (Al_3Li), δ (AlLi), S'' (Al_2CuMg), T_1 (Al_2CuLi) and β' (Al_3Zr), that are present in the alloy system. TEM and DSC studies have confirmed that retrogression causes dissolution of δ' into matrix and reaging the retrogressed state causes reprecipitation of δ' phase within the matrix. Retrogression treatment results in decrease of hardness and tensile strength and an increase of ductility, which is attributed to the dissolution of matrix strengthening δ' precipitates. Dissolution of δ' precipitates also causes a reduction of planar slip contributing to an increase of ductility of the retrogressed temper. The observation of serration in the stress–strain curves of the retrogressed state is attributed to work softening on account of slip localization (due to less volume fraction of δ' phase in the matrix) and interaction between the diffusing solute atoms and mobile dislocations. Reprecipitation of δ' phase upon reaging the retrogressed state results in regaining the original T8 hardness and tensile strength. SEM fractographs of the alloy of various tempers reveal primarily intergranular cracking and the presence of few dimples.

The authors gratefully acknowledge the help of Mr. Samar Das, National Metallurgical Laboratory, Jamshedpur in TEM studies. The authors would like to thank Dr. A. A. Gokhale and Dr Vijaya Singh, Defence Metallurgical Research Laboratory, Hyderabad, India for providing the aluminium-lithium alloy.

References

[1] J.R. Davis, in: Davis and Associates (Eds.), ASM Specialty Handbook, Aluminum and Lithium alloys, Ohio, ASM International (1998).
[2] E.A. Starke Jr., T.H. Sanders Jr., in: Engineering Materials Advisory Services (Ed.), Proc. 1st Int. Conf. on Aluminum alloys: Their Physical and Mechanical Properties; England (1986).
[3] S.J. Harris, B. Noble, K. Dinsdale, in: T.H. Sanders Jr., E.A. Starke Jr. (Eds), Proc. 2nd Int. Conf. on Aluminium-Lithium alloys II, TMS, Warrendale, PA (1983) 219.
[4] A.F. Smith, in: G. Champier, B. Dubost, D. Miannay, L. Sabetay (Eds.), Proc. 4th Int. Conf. on Aluminium-Lithium alloys IV, Paris, June, 1987, J. de Phys Colloque, 48 (1987) C3: 49.
[5] K.T. Vekateswara Rao, W. Yu, R.B. Ritchie: Metal. Trans. A 19 (1988) 563.
[6] W.S. Miller, J. White, D.J. Lloyd, in: G. Champier, B. Dubost, D. Miannay, L. Sabetay (Eds.), Proc. 4th Int. Conf. on Aluminium-Lithium alloys IV, Paris, J. de Phys Colloque, 48 (1987) C3: 139.
[7] F. Binsfeld, M. Habashi, J. Galland, J.P. Fidelle, D. Miannay, P. Rofidal, in: G. Champier, B. Dubost, D. Miannay, L. Sabetay (Eds.), Proc. 4th Int. Conf. on Aluminium-Lithium alloys IV, Paris, J. de Phys Colloque 48 (1987) C3: 587.
[8] B. Cina, B. Ranish: Paper No. XXV, Aluminium Industrial Products, ASM, Pittsburg, PA, October, 1974.
[9] B. Cina: US Patent No. 3856584, December 24, 1974.
[10] N.J.H. Holroyd, A. Gray, G.M. Scamans, R. Herman: Proc. 3rd Int. Conf. on Aluminum Lithium Alloys III, The Inst. Metals, London (1986) 310.
[11] A. Conde, J.J. Damaborenea: Corrosion Science 41 (1999) 1079.
[12] A. Gray, in: G. Champier, B. Dubost, D. Miannay, L. Sabetay (Eds.), Proc. 4th Int. Conf. on Aluminium-Lithium alloys IV, Paris, J. de Phys Colloque 48 (1987) C3: 891.
[13] X. Xiaoxin, J.W. Martin, in: G. Champier, B. Dubost, D. Miannay, L. Sabetay (Eds.), Proc. 4th Int. Conf. on Aluminium-Lithium alloys IV, Paris, J. de Phys Colloque, 48 (1987) C3: 433.
[14] P.C. Mckeighan, J.A. Henkener, G.P. Kistler, T.H. Sanders Jr., A.F. Grandt Jr., B. Hillberry, in: G. Champier, B. Dubost, D. Miannay, L. Sabetay (Eds.), Proc. 4th Int. Conf. on Aluminium-Lithium alloys IV, Paris, J. de Phys Colloque 48 (1987) C3: 849.
[15] Z.Q. Zhou, X. He, D.X. Ji, C.Q. Chen, in: G. Champier, B. Dubost, D. Miannay, L. Sabetay (Eds.), Proc. 4th Int. Conf. on Aluminium-Lithium alloys IV, Paris, J. de Phys Colloque 48 (1987) C3: 879.
[16] S. Fox, H.M. Flower, D.C. McDarmaid, in: C. Baker, P.J. Gregson, S.J. Harris, C.J. Peel (Eds.), Proc. 3rd Int. Conf. on Aluminium-Lithium Alloys, The Institute of Metals, London (1986) 263.
[17] K. Satyaprasad, A.A. Gokhale, A.A. Mukhopadhyay, D. Banerjee, D.B. Goel: Acta mater. 47 (1999) 2581.
[18] P. Gomiero, F. Livet, Y. Brechet, D.F. Louchet: Acta. metall. mater. 40 (1992) 847.
[19] A.K. Gupta, P. Gaunt, M.C. Chaturvedi: Phil. Mag. 55 (1987) 375.
[20] K. Satyaprasad, A.K. Mukhopadhyay, D. Banerjee, D.B. Goel: Scr. Metall. 30 (1994) 1299.

[21] K.S. Ghosh, K. Das, U.K. Chatterjee: Metal and Mater. Trans. A 35 (2004) 3681.
[22] K.S. Ghosh, K. Das, U.K. Chatterjee: Mater. Sci. and Techn. 20 (2004) 825.
[23] A.K. Mukhopadhyay, C.N.J. Tite, H.M. Flower, P.J. Gregson, F. Sale, in: G. Champier, B. Dubost, D. Miannay, L. Sabetay, (Eds.), Proc. 4th Int. Conf. on Aluminium Lithium Alloys, J. de Phys. Colloque 48 (1987) C3: 439.
[24] A. Luo, D.J. Lloyd, A. Gupta, W.V. Youdelis: Acta metall. mater. 41 (1993) 769.
[25] M.J Starink, A.J. Hobson, P.J. Gregson: Scripta Metall. 11 (1996) 1711.
[26] M.J. Starink, P.J. Gregson: Mater Sci. Forum, 217–222 (1996) 673.
[27] K.S. Ghosh: PhD Thesis, Indian Institute of Technology, Kharagpur, India, Oct. 2002.
[28] J.K. Park: Mater. Sci. Eng. A 103 (1988) 223.
[29] K. Rajan, W. Wallace, J.C. Beddoes: J. Mater. Sci. 17 (1982) 2817.
[30] M.U. Islam, W. Wallace: Metals Tech. 10 (1983) 386.
[31] M. Kanno, I. Araki, Q. Cui: Mater. Sci. Tech. 10 (1994) 599.
[32] M.B. Hall, J.W. Martin: Z. Metallkd. 85 (1994) 134.
[33] C. Thakur, R. Balasubramaniam: Acta mater. 45 (1997) 1323.
[34] B.S. Kaneko: Metal Progress 118 (1980) 41.
[35] T.H. Sanders, E.A. Starke Jr.: Acta metall. 30 (1982) 927.
[36] L.P. Kubin, Y. Estrin: Rev. de Phys. Appl. 23 (1988) 573.
[37] D.S. McDarmaid: Mater. Sci. and Eng. A 101 (1988) 193.
[38] P. Gomiero, Y. Brechet, F. Louchet, A. Tourabi, B. Wack: Acta metall. mater. 40 (1992) 863.
[39] K.S. Kumar, S.A. Brown, J.R. Pickens: Acta mater. 44 (1996) 1899.
[40] S. Kumar, E. Pink: Scripta metall. 33 (1995) 81.
[41] J.A. Wert, P.A. Wycliffe: Scripta metall. 19 (1985) 463.
[42] N. Ilic, D.J. Drobnjak, V. Radmilovic, M.T. Jovanovic, D. Markovic: Scripta Met. 34 (1996) 1123.
[43] R.B. Schwarz, L.L. Funk: Acta metall. 33 (1985) 295.
[44] T.S. Srivatsan, T. Alan Place: J. Mater. Sci. 24 (1989) 1543.
[45] P.J. Gregson, H.W. Flower: Acta metall. 33 (1985) 527.
[46] B. Noble, S.J. Harris, K. Dinsdale: Metall. Sci. 16 (1982) 425.
[47] E. Nembach: Progr. in Mater. Sci. 45 (2000) 275.
[48] T.H. Sanders Jr., E.A. Ludwiczak, R.R. Sawtell: Mater Sci. and Eng. 43 (1980) 247.
[49] A.K. Vasudevan, E.A. Ludwiczak, S.F. Baumann, P.R. Howell, R.H. Doherty, D.M. Kersker: Mater. Sci. and Techn. 2 (1986) 1205.

(Received April 28, 2005; accepted June 28, 2005)

Correspondence address

Dr. K. S. Ghosh
Department of Metallurgical and Materials Engineering
National Institute of Technology-Warangal
506004 Warangal, India
Tel.: +91 870 246 2520
Fax: +91 870 246 9547
E-mail: kshghosh2001@yahoo.co.uk